

# Geometrical renormalization approach to calculating optical properties of fractal carbonaceous soot

Vadim A. Markel

*Department of Electrical Engineering, Washington University, St. Louis, Missouri 63130*

Vladimir M. Shalaev

*Department of Physics, New Mexico State University, Las Cruces, New Mexico 88003*

Received June 15, 2000; revised manuscript received November 3, 2000; accepted November 8, 2000

We develop a theoretical approach to calculating optical properties of carbonaceous soot in the long-wavelength limit. Our method is based on geometrical renormalization of clusters; it avoids both the inaccuracy of the dipole approximation in its pure form and the numerical complexity of rigorous direct methods of solving the EM boundary problem. The results are verified by comparison with the experimental measurements for specific extinction of diesel soot in the spectral region from  $0.488\ \mu\text{m}$  to  $0.857\ \text{cm}$  that were performed by Bruce *et al.* [Appl. Opt. **30**, 1537 (1991)]. The theory leads to analytical expressions that are applicable to different soots, with various geometrical properties and optical constants. We show that the functional form of the long-wavelength asymptote of the specific extinction can depend critically on a parameter characterizing the sample geometry, and we identify the critical value of this parameter. © 2001 Optical Society of America  
OCIS codes: 010.1110, 290.1090, 290.2200, 290.3770.

## 1. INTRODUCTION

### A. Review of the Problem

Understanding the optical properties of carbonaceous soot in a wide spectral range is important for many areas of application such as climate research, monitoring of atmospheric pollution, and remote sensing of fires. It has long been recognized<sup>1-4</sup> that aerosol soot consists of fractal clusters built of many hundreds or thousands of nanometer-scale carbon spheres (monomers), and the geometrical structure of soot plays an important role in determining the soot's optical properties. In the visible and near-infrared spectral regions the electromagnetic interaction of monomers in a soot cluster is relatively weak, and analytical perturbative approaches such as the mean-field approximation<sup>5</sup> produce sufficiently accurate results. However, as the wavelength is further increased, the optical constants of black carbon become more metalliclike (dominated by the input of conduction electrons),<sup>6</sup> which leads to stronger electromagnetic interaction and the eventual breakdown of the perturbative methods. As a result, the collective optical properties of a soot cluster become increasingly different from those of isolated monomers.<sup>7,8</sup> Experimental measurements of the absorption and extinction efficiencies of diesel soot in a very wide spectral range<sup>9</sup> ( $0.5\ \mu\text{m}$  to  $0.857\ \text{cm}$ ) have demonstrated that neither the model of isolated spheres nor that of long cylinders can explain the spectral dependence of the quantities cited above.

The nonperturbative methods that can account for strong EM interaction in the long-wavelength spectral region include the dipole approximation<sup>5,10-13</sup> and the family of rigorous numerical methods in which the field scat-

tered by each monomer is expanded into spherical harmonics up to a certain maximum order.<sup>8,14-19</sup> However, both methods have shortcomings. The dipole approximation for aggregated spheres is accurate only when the spheres are separated by distances larger than their diameters or when the EM interaction is weak (the latter situation took place, for example, as described in Ref. 5). The general nonapplicability of the dipole approximation to arrays of strongly interacting touching spheres was verified both theoretically<sup>14,15</sup> and experimentally.<sup>20</sup> A simple physical explanation of why the dipole approximation fails was provided, for example, in Ref. 20.

A rigorous numerical approach to solution of the Maxwell equations for touching spheres has been developed by various authors.<sup>8,14-19</sup> The essence of this method, which can be referred to as the coupled-multipole method, is to expand the EM field inside each sphere and the field scattered by each sphere in vector spherical harmonics and to match the boundary condition on all surfaces of discontinuity. Generally, this method leads to an infinite-dimensional system of linear equations with respect to the expansion coefficients. To solve this system, one needs to truncate it by assuming that all the expansion coefficients for spherical harmonics of order larger than  $L$  are zero. Then the total number of equations scales (for large values of  $L$ ) as  $NL^2$ . Although this method gives a rigorous numerical solution to the Maxwell equations in the limit  $L \rightarrow \infty$ , it has a fundamental difficulty: When the interaction of monomers in a cluster becomes stronger and the perturbation expansion, correspondingly, less accurate (or even diverges), the number  $L$  required for attaining accurate results tends to

increase.<sup>21,22</sup> This property is illustrated in Fig. 3 below. However, the number  $N$  should stay sufficiently large to retain the fractal geometry of samples.

To overcome the inadequacy of the dipole approximation and the overwhelming computational complexity of the coupled multipole method, we suggest using the geometrical cluster renormalization method (GCRM).<sup>23,24</sup> This approach allows one to stay in the frame of the dipole approximation. In this paper we focus on application of this method to carbonaceous soot in the spectral range of approximately  $0.5 \mu\text{m}$ – $1 \text{ cm}$ . The results are compared with experimental measurements reported by Bruce *et al.*<sup>9</sup>

The major advantage of the GCRM is its numerical simplicity. But, in addition, useful analytical results can be obtained in an approximation in which the retardation effects are ignored (the quasi-static limit) and the weighted density of states (WDS) of the dipole interaction operator is replaced by a step function. These two approximations lead to an analytical formula that is highly accurate (as verified by comparison with results of direct numerical calculations within the GCRM) for materials such as black carbon in the spectral range from the near IR to centimeter waves. The availability of an analytical expression allows one to investigate the dependence of the spectra on important parameters of the problem and to make conclusions of a more general applicability.

### B. Optical Constants of Black Carbon

Any numerical or analytical calculation requires knowledge of optical constants of the soot material. Unfortunately, there is some uncertainty in this matter. Black carbon can exist in several modifications (graphite, amorphous, glassy carbon). We use the data of Dalzell and Sarofim,<sup>6</sup> who proposed a three-electron dispersion formula for optical constants and verified it experimentally in the spectral range  $0.4 \mu\text{m} < \lambda < 10 \mu\text{m}$ . The availability of an analytic expression for the optical constants allowed us to extrapolate them into a much wider spectral range. The important feature of this dispersion formula is the presence of a free-electron term that dominates the optical constants at large wavelengths.

The dispersion formula for the dielectric constant  $\epsilon$  suggested by Dalzell and Sarofim is based on the well-known quantum expression for the complex dielectric function:

$$\epsilon(\omega) = 1 - \sum_n \frac{f_n^2}{\omega^2 - \omega_n^2 + i\gamma_n\omega}. \quad (1)$$

Earlier, Taft and Philipp<sup>25</sup> identified experimentally three optical resonances in graphite, two of which correspond to bound electrons and one to conduction electrons. The resonance frequencies are  $\omega_c = 0$  (conduction electrons),  $\omega_1 = 1.25 \times 10^{15} \text{ s}^{-1}$ , and  $\omega_2 = 7.25 \times 10^{15} \text{ s}^{-1}$  (or the corresponding wavelengths:  $\lambda_c = \infty$ ,  $\lambda_1 = 1.51 \mu\text{m}$ , and  $\lambda_2 = 0.26 \mu\text{m}$ ). The values of the relaxation constants were found to be  $\gamma_c = \gamma_1 = 6.00 \times 10^{15} \text{ s}^{-1}$  and  $\gamma_2 = 7.25 \times 10^{15} \text{ s}^{-1}$ . Dalzell and Sarofim<sup>6</sup> assumed that the same electronic transitions contribute to the dielectric constant of carbon soot and used the above values of  $\omega_n$  and  $\gamma_n$  to fit formula (1) to their experimental data, treating  $f_n$  (which depend on the

concentration of optically active electrons) as free parameters. A highly accurate fit to the experimental data for propane soot was achieved for the following values of  $f_n$ :  $f_c = 4.04 \times 10^{15} \text{ s}^{-1}$ ,  $f_1 = 2.93 \times 10^{15} \text{ s}^{-1}$ , and  $f_2 = 9.54 \times 10^{15} \text{ s}^{-1}$  in the spectral range  $0.4 \mu\text{m} < \lambda < 10 \mu\text{m}$ . Analogous three-electron dispersion formulas were used to describe optical constants of smoke at the flame temperatures.<sup>26</sup> The temperature dependence is governed mainly by the temperature dependence of the conduction electron relaxation constant<sup>27</sup>:  $\gamma_c \propto T^{1/2}$ .

The real and imaginary parts of the complex refractive index  $m = \sqrt{\epsilon} = n + ik$  calculated from formula (1) with the constants specified above are shown in Fig. 1. The low-frequency metallic behavior of the optical constants is clearly manifested for  $\lambda > 100 \mu\text{m}$ :  $n$  and  $k$  become very close to each other and scale with wavelength as  $\sqrt{\lambda}$ . Mathematically, this happens when the term  $if_c^2/\gamma_c\omega$  becomes dominant in formula (1), i.e., for  $\omega \ll \gamma_c$ .

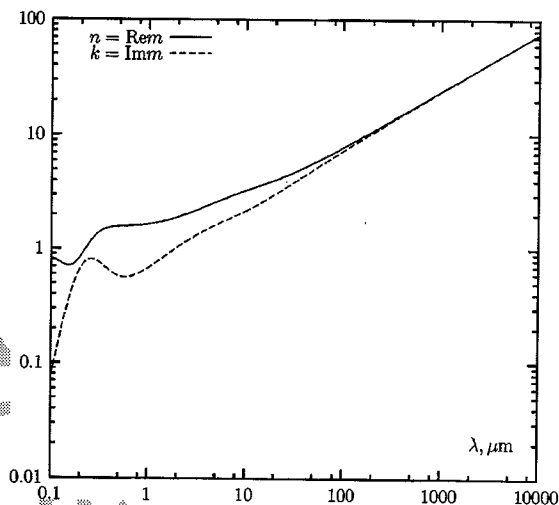


Fig. 1. Real and imaginary parts of the complex refractive index  $m = \sqrt{\epsilon} = n + ik$  as functions of wavelength calculated from dispersion formula (1).

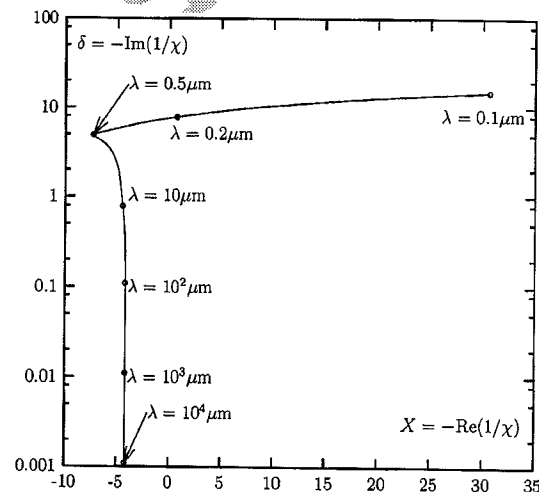


Fig. 2. Spectral dependence of complex variable  $1/\chi = -(X + i\delta)/(\epsilon + 2)$  parameterized by wavelength  $\lambda$ , where  $\chi = (3/4\pi)(\epsilon - 1)/(\epsilon + 2)$ .

In Fig. 2 we show the spectral dependence of two important optical parameters,  $X$  and  $\delta$ , originally introduced<sup>28</sup> in Refs. 10 and 11. They are defined as  $X = -\text{Re}(1/\chi)$  and  $\delta = -\text{Im}(1/\chi)$ , where

$$\chi = \frac{3}{4\pi} \frac{\epsilon - 1}{\epsilon + 2}. \quad (2)$$

The physical meaning of these parameters is that  $X$  is the generalized detuning from resonance and  $\delta$  is the generalized dielectric loss parameter.

### C. Convergence of the Coupled-Multipole Method

The breakdown of the dipole approximation for clusters of touching spheres happens even when the overall size of the clusters is much smaller than the wavelength, and the usual quasi-static methods apply.<sup>8,29</sup> In principle, this problem can be resolved by using rigorous numerical solution to the Maxwell equations.<sup>8,14,29</sup> However, the convergence of these methods with the maximum order of spherical harmonics used ( $L$ ) is a major problem for large clusters. The number of linear equations that must be solved in this approach scales as  $NL^2$ , where  $N$  is the number of primary spheres. In this subsection we demonstrate that such convergence cannot be realistically achieved for  $\lambda > 10 \mu\text{m}$ .

We used in our calculations a model fractal cluster of  $N = 100$  primary spheres. The cluster was generated by the cluster-cluster aggregation process<sup>30,31</sup> in three dimensions. We calculated the specific extinction  $\epsilon_e$  (per unit volume), defined as

$$\epsilon_e = \frac{\sigma_e}{V_{\text{tot}}}, \quad (3)$$

where  $\sigma_e$  is the total extinction cross section and  $V_{\text{tot}}$  is the total volume of the cluster (equal to  $N$  times the volume of primary spheres,  $v$ ). Quasi-static Fortran codes courtesy of D. W. Mackowski were used in the calculations (see Refs. 8 and 29 for more details), and the refractive index was calculated with formula (1).

The results are presented in Fig. 3, where we plot the quantity  $\lambda^2 \epsilon_e$  as a function of  $L$  for several wavelengths. The specific extinction is multiplied by  $\lambda^2$  so that the data for several values of  $\lambda$  can all be compared in the same plot. It can be seen that a fast convergence is reached for  $\lambda = 1 \mu\text{m}$ . (The scale of this figure does not allow one to see that convergence is, in fact, achieved for  $L > 4$  at this wavelength.) The convergence for  $\lambda = 10 \mu\text{m}$  is somewhat slower. It is, actually, difficult to judge from the figure if the result can still change considerably with increasing  $L$ .

But, for the wavelengths  $\lambda = 10^2, 10^3$ , and  $10^4 \mu\text{m}$ , when the refractive index of carbon is metallic (see Fig. 1), convergence is not achieved at all. The quantity  $\lambda^2 \epsilon_e$  grows linearly with  $L$  and does not depend noticeably on  $\lambda$ . Extrapolating the linear growth of  $\lambda^2 \epsilon_e$  to larger values of  $L$ , and using experimental values of the specific extinction, we can roughly estimate the lower bound of  $L$  that is required for convergence. From experimental data of Bruce *et al.*<sup>9</sup> we find that  $\epsilon_e \approx 0.13 \mu\text{m}^{-1}$  for  $\lambda \approx 100 \mu\text{m}$ . (To obtain this result, we used the mass density of black carbon,  $\rho \approx 2 \text{ g/cm}^3$ ; specific extinction in

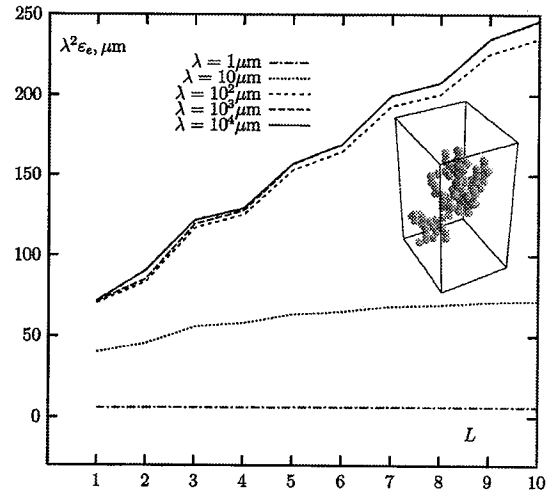


Fig. 3. Specific extinction  $\epsilon_e$ , multiplied by  $\lambda^2$  and averaged over spatial rotations, as a function of  $L$  (Fortran codes courtesy of D. Mackowski). The calculations were performed in the quasi-static limit for a three-dimensional cluster-cluster aggregate of  $N = 100$  touching spheres as shown in the inset.

Ref. 9 is measured per unit of mass rather than of volume.) Thus, at  $\lambda \approx 100 \mu\text{m}$ , we have  $\lambda^2 \epsilon_e \approx 1300 \mu\text{m}$ . The linear growth of  $\lambda^2 \epsilon_e$  as a function of  $L$  in Fig. 3 can be approximated by  $\lambda^2 \epsilon_e = [50 + 20L] \mu\text{m}$ . If this linear behavior is extrapolated to larger values of  $L$ , the experimental value of  $\lambda^2 \epsilon_e$  is reached at  $L \approx 65$ . However, it is plausible to assume that the slope of the curve  $\lambda^2 \epsilon_e(L)$  will decrease for larger  $L$  and that the actual number of spherical harmonics necessary for convergence is larger than 65. Even for  $L \approx 65$  and  $N = 100$ , the number of equations that must be solved is 422,500. And a larger  $L$  is required for  $\lambda > 100 \mu\text{m}$ . This makes the direct numerical approach impractical for large wavelengths.

It can be seen from Fig. 3 that the dependence  $\epsilon_e(L)$  has the form of a ladder with alternating steps of different heights. For example,  $\epsilon_e(4) - \epsilon_e(3)$  is much smaller than  $\epsilon_e(5) - \epsilon_e(4)$ . Therefore, it is generally incorrect to stop iterations at a certain value of  $L$  when the change in  $\epsilon_e$  is less than some small constant. Instead, this condition should hold for two consecutive iterations. Also, even if the above condition is met, it is not always clear that a relatively large change in  $\epsilon_e$  will not accumulate for larger values of  $L$ . Thus the convergence criterion should be not the small change in  $\epsilon_e$  after two consecutive iterations but rather a manifested plateau in the curve  $\epsilon_e(L)$ .

## 2. THEORY

### A. Dipole Approximation

In this subsection we briefly describe the dipole approximation in its generic form and introduce the relevant notation.

The essence of the dipole approximation is to replace each (finite-size) monomer in a cluster by a point dipole with polarizability  $\alpha_i$ , located at point  $\mathbf{r}_i$  at the center of the respective spherical monomer. The dipole moment of

the  $i$ th monomer,  $\mathbf{d}_i$ , is proportional to the local field at point  $\mathbf{r}_i$ , which is a superposition of the incident field and all the secondary fields scattered by other dipoles. Therefore the dipole moments of the monomers are coupled to the incident field and to each other as described by the coupled-dipole equation

$$\mathbf{d}_i = \alpha \left[ \mathbf{E}_{\text{inc}}(\mathbf{r}_i) + \sum_{j \neq i}^N \hat{G}(\mathbf{r}_i - \mathbf{r}_j) \mathbf{d}_j \right], \quad (4)$$

where the term  $\hat{G}(\mathbf{r}_i - \mathbf{r}_j) \mathbf{d}_j$  gives the dipole radiation field created by dipole  $\mathbf{d}_j$  at point  $\mathbf{r}_i$  and  $\hat{G}(\mathbf{r})$  is the regular part of the free-space dyadic Green's function:

$$G_{\alpha\beta}(r) = k^3 [A(kr) \delta_{\alpha\beta} + B(kr) r_\alpha r_\beta / r^2], \quad (5)$$

$$A(x) = (x^{-1} + ix^{-2} - x^{-3}) \exp(ix), \quad (6)$$

$$B(x) = (-x^{-1} - 3ix^{-2} + 3x^{-3}) \exp(ix), \quad (7)$$

where  $k = 2\pi/\lambda$  is the wave number,  $(\hat{G}\mathbf{d})_\alpha = G_{\alpha\beta} d_\beta$ , the greek subscripts stand for the Cartesian components of vectors, and summation over repeated indices is implied.

The coupled-dipole equation is a system of  $3N$  linear equations that one can solve to find dipole moments  $\mathbf{d}_i$ . The cross sections of extinction and absorption can be found from the optical theorem

$$\sigma_e = \frac{4\pi k}{|\mathbf{E}_0|^2} \text{Im} \sum_{i=1}^N \mathbf{d}_i \cdot \mathbf{E}_{\text{inc}}^*(\mathbf{r}_i), \quad (8)$$

$$\sigma_a = \frac{4\pi k}{|\mathbf{E}_0|^2} y_a \sum_{i=1}^N |\mathbf{d}_i|^2, \quad (9)$$

$$y_a = -\text{Im} \left( \frac{1}{\alpha} \right) - \frac{2k^3}{3} \geq 0. \quad (10)$$

For monomers small compared with  $\lambda$ , polarizability  $\alpha$  is given by<sup>32</sup>

$$\frac{1}{\alpha} = \frac{1}{v\chi} - i \frac{2k^3}{3}, \quad (11)$$

where  $v = (4\pi/3)R_m^3$  is the volume of a spherical monomer,  $R_m$  is its radius, and the susceptibility  $\chi$  is defined by formula (2). As follows from formulas (10), (11) and (2),  $y_a$  is nonnegatively defined for any physically reasonable  $\epsilon$ . The ratio  $3y_a/2k^3$  characterizes the relative strength of absorption by a single isolated monomer.

## B. Geometrical Renormalization of Clusters

In this subsection we describe the GCRM and its application in the dipole approximation.

First, we note that most calculations employ computer-generated samples. The geometry of these samples does not coincide exactly with that of experimental soot (which is, obviously, impossible) but rather reproduces certain statistical geometrical properties of the real soot. Among such properties are density correlation functions; total volume of the material,  $V_{\text{tot}} = Nv$ ; and average radius of gyration,  $R_g$ . However, such characteristics as the number of monomers in a cluster,  $N$ , and monomer radius,

$R_m$ , might be considered not essential. It is known, for example, that the real carbon monomers are not actually spherical and that nearest neighbors touch each other not just at one geometrical point, so the model of touching spheres is only an idealization.

Second, as was mentioned above, the dipole approximation in its pure form underestimates the strength of electromagnetic interactions between the monomers. In particular, it predicts that the shift of the resonance frequency in small clusters of spheres will be significantly less than that experimentally measured.<sup>20</sup> To correct the interaction strength of the dipole approximation, we can move the monomers closer to one another (of course, this refers to computer-generated samples) by allowing them to intersect geometrically. However, doing this will evidently reduce the overall system size ( $R_g$ ), which is an essential parameter of the problem. The other possible way to introduce the intersections is to increase the radii of the spheres ( $R_m$ ) while keeping the distance between nearest neighbors ( $l$ ) unchanged. Doing so will, however, lead to an increase of the total volume of the material. Luckily, for fractal clusters it is possible to introduce a simultaneous renormalization of the sphere radii ( $R_m$ ), the total number of monomers ( $N$ ) and the distance between the nearest neighbors ( $l$ ) in such a way that the overall volume ( $V_{\text{tot}}$ ) and the gyration radius ( $R_g$ ) are unchanged and to introduce an arbitrary geometrical intersection of neighboring spheres. The transformation is

$$R_m' = R_m (\xi/2)^{D/(3-D)}, \quad (12)$$

$$N' = N(2/\xi)^{3D/(3-D)}, \quad (13)$$

$$l' = \xi R_m', \quad (14)$$

where  $\xi$  is an intersection parameter ( $1 < \xi < 2$ ;  $\xi = 2$  for touching spheres and  $\xi < 2$  for geometrically intersecting spheres). Indeed, it is easy to verify that the gyration radius, which scales with  $l$  and  $N$  as

$$R_g \propto lN^{1/D}, \quad (15)$$

and the total volume, which scales with  $R_m$  and  $N$  as

$$V_{\text{tot}} \propto NR_m^3, \quad (16)$$

do not change under the set of transformations defined by formulas (12)–(14).

Thus the main idea of the renormalization approach is to model an ensemble of real clusters with experimental values of  $R_m$  and  $N$  and  $l = 2R_m$  by a computer-generated renormalized ensemble with corresponding parameters  $R_m'$  and  $N'$ , and with the geometrical intersection of neighboring spheres:  $l' = \xi R_m' < 2R_m'$ . It is important to emphasize that the renormalization does not apply to a single random cluster (because it changes not only the interparticle separation but also the number of particles in an individual cluster) but is rather an operation that creates the renormalized random ensemble for a given original (experimental) ensemble.

The initial value for  $\xi$  can be obtained by analogy with the discrete-dipole approximation (see Refs. 32–34) in which bulk nonspherical particles are modeled by arrays of point dipoles located on a cubic lattice. In the first approximation, the polarizability of the dipoles is taken to be equal to that of an equivalent sphere with the radius

$R_m$  such that its volume is equal to the volume of a lattice cell, i.e.,  $(4\pi/3)R_m^3 = l^3$ . From this equality we find that  $\xi = l/R_m = (4\pi/3)^{1/3} \approx 1.612$ .

Another approach to estimating parameter  $\xi$  is based on the following consideration which can also be used to justify the physical plausibility of the renormalization method. It can be shown<sup>35</sup> that a linear chain of intersecting spheres has the same depolarization coefficients as an infinite cylinder (within the dipole approximation)<sup>36</sup> for  $\xi = [4 \sum_{k=1}^{\infty} k^{-3}]^{1/3} \approx 1.688$ . This value is close to the one obtained above. It is important to note that two independent depolarization coefficients can simultaneously be tuned to correct values by adjusting only one free parameter  $\xi$ . As is well known, the depolarization coefficients in ellipsoids (an infinite cylinder is a particular case) determine the spectral positions of the resonances. Thus the renormalization procedure gives the correct spectral locations of the optical resonances for a one-dimensional chain. The line shape of each resonance can still be described incorrectly. However, in the situation of a large fractal cluster, typical absorption and extinction spectra are superpositions of many collective resonances, and the line shapes of individual resonance are of little importance.

### C. Quasi-Static Limit

The quasi-static limit plays an important role in the long-wavelength electromagnetic properties of soot. This approximation is highly accurate in the spectral range under consideration ( $0.6 \mu\text{m} < \lambda < 1 \text{ cm}$ ) and provides valuable mathematical simplifications.

When the wavelength is much larger than all characteristic sizes of the system, the terms proportional to  $x^{-1}$  and  $x^{-2}$  in Eqs. (6) and (7) can be omitted,  $\exp(ix)$  set to unity, and the incident wave on the right-hand side of Eq. (4) replaced by a constant field  $\mathbf{E}_0$ . The resultant equation can be written in operator form as

$$|d\rangle = \alpha(|E_{\text{inc}}\rangle + W|d\rangle), \quad (17)$$

where  $|d\rangle$  is the  $3N$ -dimensional vector of dipole moments with components  $\langle i\alpha|d\rangle = d_{i\alpha}$ , and, analogously,  $|E_{\text{inc}}\rangle$  is the vector of the incident fields with  $\langle i\alpha|E_{\text{inc}}\rangle = E_{0\alpha}$ . The  $3N \times 3N$ -dimensional operator  $W$  is real and symmetric in the quasi-static limit and therefore is Hermitian. Its matrix elements are given by

$$\langle i\alpha|W|i\beta\rangle = -\frac{\delta_{\alpha\beta}}{|\mathbf{r}_i - \mathbf{r}_j|^3} + \frac{3(\mathbf{r}_i - \mathbf{r}_j)_\alpha(\mathbf{r}_i - \mathbf{r}_j)_\beta}{|\mathbf{r}_i - \mathbf{r}_j|^5}. \quad (18)$$

Equation (17) can be formally solved by use of the spectral theorem as<sup>10,11</sup>

$$|d\rangle = \sum_n \frac{|n\rangle\langle n|E_{\text{inc}}\rangle}{1/\alpha - w_n}, \quad (19)$$

where  $|n\rangle$  are the eigenvectors of  $W$  with corresponding eigenvalues  $w_n$ . The expression for the extinction cross section [Eq. (8)] takes the form

$$\sigma_e = \frac{4\pi k}{|\mathbf{E}_0|^2} \text{Im}\langle E_{\text{inc}}|d\rangle = \frac{4\pi k v}{|\mathbf{E}_0|^2} \text{Im} \sum_n \frac{\langle E_{\text{inc}}|n\rangle\langle n|E_{\text{inc}}\rangle}{1/\chi - v w_n}, \quad (20)$$

where we have used Eq. (11) for  $1/\alpha$  and neglected, in the quasi-static limit, the term  $2k^3/3$ .

In the limit  $k \rightarrow 0$ , Eqs. (8) and (9) are exactly equal.<sup>10,11</sup> Therefore the scattering cross section is zero in this limit. However,  $\sigma_s$  can be calculated in a higher-order perturbation expansion, where  $2k^3/3$  is considered to be a small parameter. If there are no antisymmetrical states in the system,<sup>37,38</sup> or if the absorption parameter  $3y_a/2k^3$  is large, the integral scattering cross section is given by

$$\sigma_s = \frac{8\pi k^4}{3|\mathbf{E}_0|^2} |\mathbf{D}|^2, \quad (21)$$

where  $\mathbf{D} = \sum_i \mathbf{d}_i$  is the total dipole moment of a cluster. The above conditions typically hold for carbon soot clusters. For example, for  $\lambda = 1 \text{ cm}$  and  $R_m = 50 \text{ nm}$  we have  $3y_a/2k^3 \approx 10^{10}$ . This result allows us to use Eq. (21), which implies that the whole cluster radiates as a single dipole.

One can obtain the expression for  $|\mathbf{D}|^2$  by using the homogeneous vectors  $|O_\alpha\rangle$  with components  $\langle i\beta|O_\alpha\rangle = \delta_{\alpha\beta}$  by observing that  $D_\alpha = \langle O_\alpha|d\rangle$ , which leads to

$$\sigma_s = \frac{8\pi k^4 v^2}{3|\mathbf{E}_0|^2} \sum_{\alpha, m, n} \frac{\langle E_{\text{inc}}|m\rangle\langle m|O_\alpha\rangle\langle O_\alpha|n\rangle\langle n|E_{\text{inc}}\rangle}{(1/\chi^* - v w_m)(1/\chi - v w_n)}. \quad (22)$$

### D. Weighted Density of States and the Step-Function Approximation

In the quasi-static limit one can average the extinction cross section over spatial rotations of a cluster by taking the arithmetic average of the corresponding expressions for three orthogonal polarizations of the incident field.<sup>10,11</sup> Mathematically, this can be expressed as

$$\bar{\sigma}_e = \frac{4\pi k v}{3} \text{Im} \sum_{n, \alpha} \frac{\langle O_\alpha|n\rangle\langle n|O_\alpha\rangle}{1/\chi - v w_n}, \quad (23)$$

where the overbar denotes rotational averaging. Now we introduce the WDS  $\Gamma_{\alpha\beta}(w)$  and  $\Gamma(w)$  according to

$$\Gamma_{\alpha\beta}(w) = \frac{1}{N} \sum_n \langle O_\alpha|n\rangle\langle n|O_\beta\rangle \delta(w - w_n), \quad (24)$$

$$\Gamma(w) = \frac{1}{3} \sum_\alpha \Gamma_{\alpha\alpha}(w). \quad (25)$$

Then Eq. (23) can be written as

$$\bar{\sigma}_e = 4\pi k V_{\text{tot}} \text{Im} \int_{-\infty}^{\infty} \frac{\Gamma(w) dw}{1/\chi - v w}. \quad (26)$$

Analogously, the expression for the scattering cross section averaged over rotations can be written in terms of the WDS as

$$\bar{\sigma}_s = \frac{8\pi k^4 V_{\text{tot}}^2}{9} \sum_{\alpha\beta} \int_{-\infty}^{\infty} \frac{\Gamma_{\beta\alpha}(w_1)\Gamma_{\alpha\beta}(w_2) dw_1 dw_2}{(1/\chi^* - v w_1)(1/\chi - v w_2)}. \quad (27)$$

The normalization rules for the WDS are

$$\int_{-\infty}^{\infty} \Gamma_{\alpha\beta}(w) dw = \delta_{\alpha\beta}. \quad (28)$$

For clusters that are, on average, spherically symmetrical, we can assume that, in the first approximation,  $\Gamma_{\alpha\beta}(w) = \delta_{\alpha\beta}\Gamma(w)$ . Then Eq. (26) becomes

$$\bar{\sigma}_s = \frac{8\pi k^4 V_{\text{tot}}^2}{3} \left| \int_{-\infty}^{\infty} \frac{\Gamma(w) dw}{1/\chi - vw} \right|^2. \quad (29)$$

The WDS calculated for an ensemble of 10 random cluster-cluster aggregates with  $N = 1000$  particles in each aggregate and fractal dimension  $D \approx 1.8$  is shown in Fig. 4 as a function of the dimensionless variable  $vw$ . The solid curve was obtained by exact diagonalization of  $W$  [Eq. (18)] and smoothing  $\Gamma(w)$  over small intervals  $\Delta w$ . The dashed line is the step-function approximation of the WDS, which is discussed in detail below.

By comparing Figs. 4 and 2, we see that the spectral variable  $1/\chi$  does not effectively probe the detailed structure of  $\Gamma(w)$  when we tune  $\lambda$ . This indicates that the complicated structure of  $\Gamma(w)$  with multiple maxima and minima is of little importance. In the simplest case, one can replace  $\Gamma(w)$  by a delta function, which is equivalent to making the mean-field approximation. However, the mean-field approximation is inaccurate in the long-wavelength limit because the variable  $1/\chi$  approaches the real axis for  $\lambda > 10 \mu\text{m}$  and the distance  $|1/\chi - vw|$  becomes comparable with the effective width of  $\Gamma(w)$ .

The next level of approximation is to replace  $\Gamma(w)$  by a step function. Such an approximation is shown in Fig. 4 by the dashed line, which preserves the normalization and the first and second moments of the exact WDS. Note also that the third moment of  $\Gamma(w)$  was numerically found to be very small, so the step function shown in Fig. 4 effectively conserves the third moment too. Here the constant  $vw_0$  was numerically estimated to be  $vw_0 \approx 2.29$ , and  $\Gamma_0 = 1/2w_0$ . The quantity  $vw_0$  is indepen-

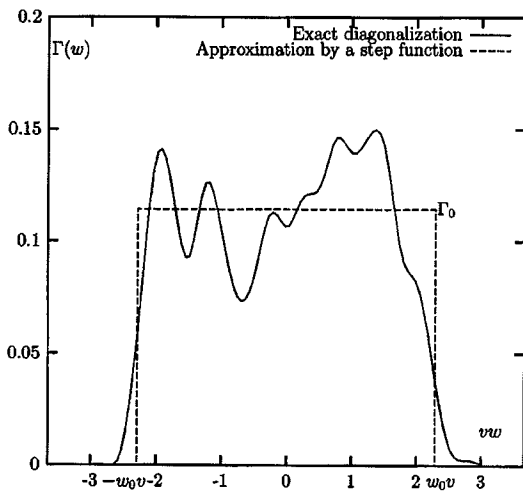


Fig. 4. Weighted density of states  $\Gamma(w)$  and its approximation by a step function with the equivalent normalization, first and second moments. The numerical diagonalization was performed for an ensemble of 10 clusters with  $N = 1000$ . The values of the constants are  $vw_0 = 2.29$  and  $\Gamma_0 = 1/2w_0$ .

dent of the system dimensions (such as  $R_m$  and  $l$ ), as one could expect in the quasi-static limit.

Given the step-function approximation for the WDS, it is easy to obtain analytical expressions for the optical cross sections. A direct integration according to Eqs. (26) and (29) yields, for the extinction and scattering cross sections,

$$\bar{\sigma}_e = \frac{2\pi k V_{\text{tot}}}{vw_0} \left( \arctan \frac{X + vw_0}{\delta} - \arctan \frac{X - vw_0}{\delta} \right), \quad (30)$$

$$\bar{\sigma}_s = \frac{2\pi k^4 V_{\text{tot}}^2}{3(vw_0)^2} \left[ \frac{1}{4} \ln^2 \frac{(X + vw_0)^2 + \delta^2}{(X - vw_0)^2 + \delta^2} + \left( \arctan \frac{X + vw_0}{\delta} - \arctan \frac{X - vw_0}{\delta} \right)^2 \right]. \quad (31)$$

Now we discuss renormalization of the parameters  $v$  and  $w_0$  under the set of transformations defined by Eqs. (12)–(14). It is easy to see that the renormalized volume is  $v' = v(\xi/2)^{3D/(3-D)}$ . In general, the eigenvalues of the interaction operator  $W$  do not scale with the parameter  $l$ , and it is impossible to write a similar relation between  $w_n$  and  $w_n'$ ; however, it does become possible in the quasi-static limit. Then, from quasi-static expression (18), it follows that  $w_n' = w_n(l/l')^3 = w_n(2/\xi)^{9/(3-D)}$ . Combining these two expressions, we obtain  $v'w_n' = vw_n(2/\xi)^3$ . Therefore the same transformation applies to  $vw_0$ :  $v'w_0' = vw_0(2/\xi)^3$ . As could be expected, this transformation does not depend on fractal dimension  $D$ . However, the dependence on  $D$  and other geometrical characteristics of a cluster is retained in the eigenvalues calculated before the renormalization, i.e., in the constant  $vw_0$ . Thus the intersection procedure effectively increases the normalized eigenvalues and, consequently, the interaction strength. The same tendency holds beyond the quasi-static limit, although the ratio  $v'w_n'/vw_n$  becomes different for different  $n$  in this case.

In summary, to use the GCRM we simply have to replace the constant  $vw_0$  in Eqs. (30) and (31) by  $vw_0(2/\xi)^3$ , where  $vw_0$  must be calculated numerically before the renormalization in an ensemble of clusters of touching spheres (i.e., with  $l = 2R_m$ ). The constant  $vw_0$  carries essential information about the cluster geometry. For the cluster-cluster aggregates generated in the Meakin model<sup>30,31</sup> with mass-independent subcluster mobility we estimated that  $D \approx 1.8$  and  $vw_0 \approx 2.29$ . It is well known that the fractal dimension can depend on the details of the aggregation process. In particular, the dependence of mobility of subclusters on their mass can influence  $D$ . In the limiting case when only subclusters built of just one monomer can move (the Witten-Sander model<sup>39</sup>), a fixed center of aggregation is formed and the fractal dimension is  $D \approx 2.5$  (for clusters embedded in three-dimensional space). We expect that the constant  $vw_0$  will also depend on the details of aggregation. Further investigation is needed to establish the dependence of  $vw_0$  on the aggregation model and whether there is a one-to-one correspondence between  $vw_0$  and  $D$ .

### 3. RESULTS

#### A. Numerical Calculations and Comparison with Experiment

To verify the validity of analytical Eqs. (30) and (31) we generated on a computer an ensemble of 10 cluster-cluster aggregates with  $N = 1000$  in each on a simple cubic lattice. We diagonalized quasi-static interaction matrix  $W$  [Eq. (18)] and calculated the extinction and scattering cross sections according to Eqs. (20) and (22). The results were averaged over cluster orientations as described in Subsection 2.D. We used the GCRM with  $\xi = (4\pi/3)^{1/3} \approx 1.612$ . The constants  $R_m$  and  $l$  were renormalized according to Eqs. (12) and (14). Note that the specific extinction  $\varepsilon_e$  depends in the quasi-static limit not on the absolute values of  $R_m$  and  $l$  but only on their ratio; the same is true for the specific scattering  $\varepsilon_s$  normalized by  $k^3 V_{\text{tot}}$ . It has also been verified<sup>23</sup> that  $\varepsilon_e$  only weakly depends on  $N$  and, therefore, on  $V_{\text{tot}}$  in the quasi-static limit, as long as  $N$  is large enough for the fractal geometry to be manifested. Because such is the case for  $N = 1000$ , there was no need to renormalize the constant  $N$  according to Eq. (13). [We emphasize that this is valid only in the quasi-static limit. The GCRM is more general and can be used beyond the quasi-statics, in which case the dependence on  $N$  can be nontrivial and all three renormalization formulas (12)–(14) must be used simultaneously.]

The results for the specific extinction  $\varepsilon_e$  and normalized specific scattering  $\varepsilon_s/k^3 V_{\text{tot}}$  are shown in Figs. 5 and 6, respectively. For comparison, we also plot in these figures the corresponding values for unaggregated particles (or in the noninteracting limit):  $\varepsilon_e^{(\text{noninteracting})} = 4\pi k \text{Im} \chi$  and  $\varepsilon_s^{(\text{noninteracting})}/k^3 V_{\text{tot}} = (8\pi/3)k|\chi|^2$ . Note that the same noninteracting expressions can be obtained in the Rayleigh-Gans (or, equivalently, the first Born) approximation. The excellent agreement between numerical and analytical results (with the interactions included) is apparent. At the same time, the noninteracting approximation is seen to become increasingly inaccurate when we move from the near to the far IR. A slightly less accurate fit is obtained for the specific scattering. This is explained by the fact that in the derivation of Eq. (31) we assumed that the clusters are spherically symmetrical. This is true only on average, whereas each individual cluster can deviate from the spherical symmetry. As a result, the off-diagonal terms in Eq. (27), which are neglected in the further derivations, are not exactly zero.

In Fig. 7 we compare analytical formula (30) with the experimental measurements of the specific extinction by Bruce *et al.*<sup>9</sup> Again, the curve that illustrates the noninteracting limit is also shown for comparison. The experimental data in Ref. 9 are given per unit of mass rather than of volume. We treated the mass density of black carbon  $\rho$  as an adjustable parameter and found that the best fit (excluding the last experimental point at  $\lambda = 8750 \mu\text{m}$ ) is achieved for  $\rho \approx 1.9 \text{ g/cm}^3$ . This is a reasonable estimate, although the experimental value of  $\rho$  in Ref. 9 is not known. (Compare this estimate with the following values: graphite,  $2.26 \text{ g/cm}^3$ ; buckminsterfullerene,  $1.69 \text{ g/cm}^3$ ; glassy carbon,  $1.42\text{--}1.54 \text{ g/cm}^3$ .) Note that  $\rho$  enters all expressions as a constant factor and does

not influence the form of the wavelength dependence of  $\varepsilon_e$ .

The surprisingly good agreement of experimental measurements with the analytical formula and the reasonable value of  $\rho$  obtained suggest that the GCRM gives accurate results for carbonaceous soot. We believe that the small deviations seen in Fig. 7 are due to insufficient accuracy of dispersion formula (1) that was used in all calculations. In particular, the apparently nonmonotonic behavior near  $\lambda = 500 \mu\text{m}$  can be explained by the presence of optical resonance at that wavelength; however, formula (1) does not contain the corresponding term. The same can be true at  $\lambda \approx 1 \text{ cm}$ , where the monotonic behavior of  $\varepsilon_e$  is again interrupted. The optical reso-

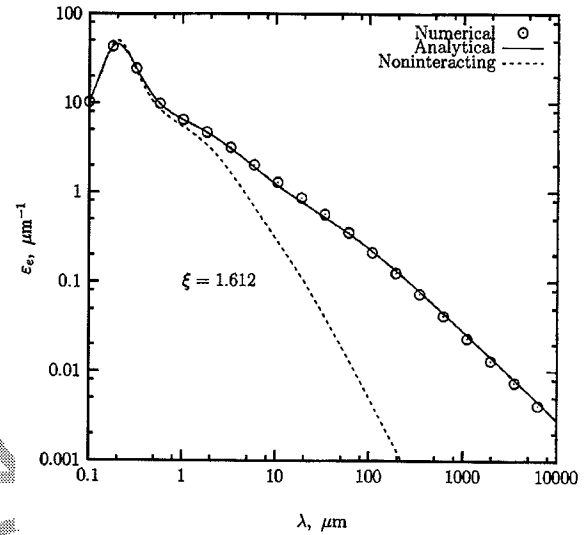


Fig. 5. Specific extinction  $\varepsilon_e$  calculated numerically (solid curve) and according to analytical approximation (30) (circles). The noninteracting limit  $\varepsilon_e^{(\text{noninteracting})} = 4\pi k \text{Im} \chi$  is shown by the dashed curve.

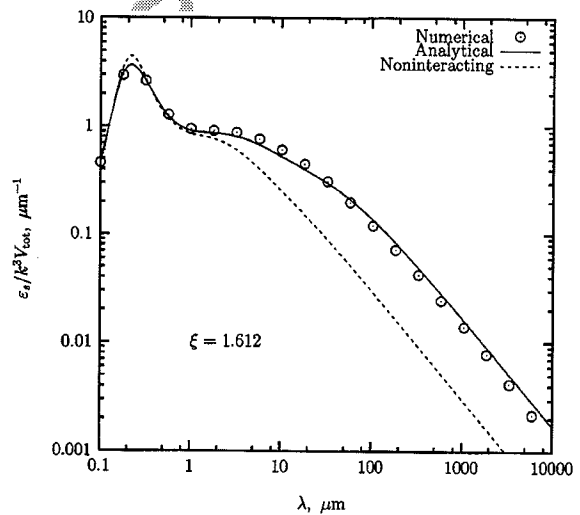


Fig. 6. Specific scattering  $\varepsilon_s$  normalized by  $k^3 V_{\text{tot}}$  calculated numerically and according to analytical approximation [Eq. (31)]. The noninteracting limit  $\varepsilon_s^{(\text{noninteracting})}/k^3 V_{\text{tot}} = (8\pi/3)k|\chi|^2$  is shown by the dashed curve.

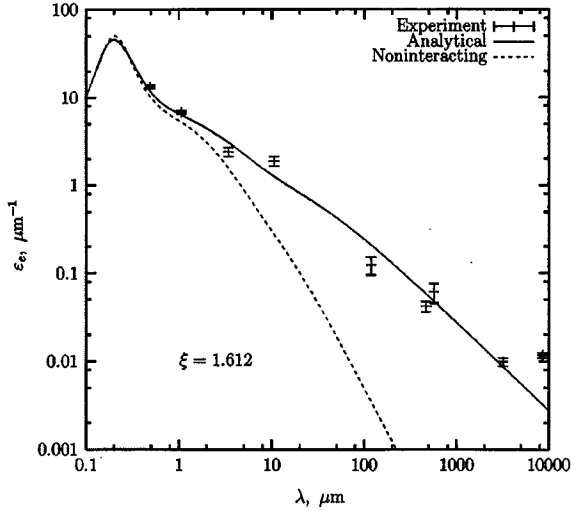


Fig. 7. Specific extinction  $\varepsilon_e$  calculated according to analytical approximation (30) compared with experimental values adapted from Bruce *et al.*<sup>9</sup> We used the mass density of black carbon,  $\rho = 1.9 \text{ g/cm}^3$ , to convert the experimental data of Ref. 9 into the units shown here. The noninteracting limit  $\varepsilon_e^{(\text{noninteracting})} = 4\pi k \text{Im} \chi$  is shown by the dashed curve.

nance at this wavelength can occur, for example, as a result of interaction with low-frequency acoustical phonons.

To conclude this section, we note that the computer-generated samples used for numerical calculation of the WDS were built on a cubic lattice. However, in real aggregates, monomers do not occupy lattice sites. The effect of using off-lattice aggregates in the computer simulations is not expected to be large and will be addressed by us in the future.

### B. Long-Wavelength Optical Properties of Soots Built from Drudean Materials

In this subsection we consider fractal clusters built of a general class of materials whose optical properties are dominated by free electrons. We have already seen that this is the case in black carbon for  $\lambda > 100 \mu\text{m}$ . We assume the idealized Drudean form of the dielectric function

$$\epsilon = 1 - \frac{\omega_p^2}{\omega(\omega + i\gamma)} \quad (32)$$

and study the asymptotic behavior of the specific extinction and scattering by using analytical expressions (30) and (31) together with the GCRM. As was discussed in Subsection 2.D, application of the GCRM results in the transformation  $\nu w_0 \rightarrow \nu w_0(2/\xi)^3$  on the right-hand sides of expressions (30) and (31). We use the notation  $C = \nu w_0(2/\xi)^3$ .

We start with the specific extinction  $\varepsilon_e = \bar{\sigma}_e/V_{\text{tot}}$ . In the limit  $\omega \rightarrow 0$ , the asymptotic values of  $X$  and  $\delta$  are

$$X = -X_\infty = -4\pi/3, \quad (33)$$

$$\delta = 4\pi\gamma\omega/\omega_p^2. \quad (34)$$

Then it follows from Eq. (30) that

$$\varepsilon_e = \frac{2\pi k}{C} \left[ \arctan \frac{C + X_\infty}{\delta} + \text{sgn}(C - X_\infty) \arctan \frac{|C - X_\infty|}{\delta} \right]. \quad (35)$$

In the limit  $\delta \ll |C - X_\infty|$ , Eq. (35) becomes

$$\varepsilon_e = \frac{2\pi k}{C} \left\{ \frac{\pi}{2} [1 + \text{sgn}(C - X_\infty)] - \delta \left[ \frac{1}{C + X_\infty} + \frac{\text{sgn}(C - X_\infty)}{|C - X_\infty|} \right] \right\}. \quad (36)$$

We can identify two separate cases: If  $C > X_\infty$ , the asymptotic form of  $\varepsilon_e$  is

$$\varepsilon_e = \frac{2\pi^2 k}{C} \propto \frac{1}{\lambda}, \quad C > X_\infty. \quad (37)$$

In the opposite case we have

$$\varepsilon_e = \frac{(4\pi)^2 \gamma k \omega}{\omega_p^2 (X_\infty^2 - C^2)} \propto \frac{1}{\lambda^2}, \quad C < X_\infty, \quad (38)$$

where we have used Eq. (34) for  $\delta$ .

We can define the critical value of the parameter  $\nu w_0$  determined by the condition  $C = X_\infty$ , or

$$(\nu w_0)_c = \frac{4\pi}{3} \left( \frac{\xi}{2} \right)^3. \quad (39)$$

If the geometry of clusters is such that  $\nu w_0 < (\nu w_0)_c$ , asymptote (38) is valid. The  $1/\lambda^2$  behavior is characteristic of noninteracting monomers (e.g., in disaggregated samples). Therefore we conclude that for  $\nu w_0 < (\nu w_0)_c$ , the EM interaction is not important in the long-wavelength regime. In the opposite case, asymptote (37) is valid, and the EM interaction remains important up to the electrostatic limit  $\omega = 0$ , which is manifested in the  $1/\lambda$  dependence.

Asymptotes (37) and (38) are valid only when  $\delta \ll |C - X_\infty|$ . If the quantity  $|C - X_\infty|$  is itself small, the asymptotic behavior of  $\varepsilon_e$  is manifested only for values of  $\lambda$  sufficiently large for the above inequality to be true. When  $C = X_\infty$ , the spectral behavior of  $\varepsilon_e$  is more complicated. In particular, higher-order terms must be retained in expression (33) for  $X$ .

In our calculations illustrated in Subsection 3.A, the numerically estimated value  $\nu w_0 \approx 2.29$  was larger than the critical value  $(\nu w_0)_c \approx 2.19$  (assuming that  $\xi = 1.612$ ). Indeed, the onset of the  $1/\lambda$  asymptote can be seen in Figs. 5–7 for  $\lambda > 100 \mu\text{m}$ . This means that in the carbon smoke with the geometry of cluster-cluster aggregates ( $D \approx 1.8$ ) and optical constants specified in Subsection 1.B, the EM interaction is always important in the long-wavelength limit. We believe that the value of  $\xi$ , and, consequently, of the critical constant  $(\nu w_0)_c$ , is universal for a broad class of soots. However, the quantity  $\nu w_0$  can depend strongly on the sample geometry. Further investigation is necessary to establish the numerical value of  $(\nu w_0)_c$  with higher accuracy and to verify the analytical results for materials with different parameters  $\nu w_0$ ,  $\gamma$ , and  $\omega_p$ .



One can obtain the mean-field approximation from Eq. (30) by considering either the limit of infinitely narrow WDS ( $w_0 \rightarrow 0$ ) or large absorption ( $\gamma \rightarrow \infty$ ). In the first case we obtain  $\varepsilon_e = 4\pi k \operatorname{Im} \chi$  and in the second case  $\varepsilon_e = 4\pi k/\delta$ . Obviously, one can obtain the latter formula from the former by taking the limit  $\delta \gg |X|$ . Note that in the quasi-static limit the mean-field and the first Born approximations are equivalent, owing to the symmetry of the dipole interaction in the near zone.

Now we turn our attention to the specific scattering,  $\varepsilon_s$ . Applying a similar analysis to Eq. (30) and assuming that  $\delta \ll |C - X_\infty|$ , we obtain

$$\frac{\varepsilon_s}{k^3 V_{\text{tot}}} = \frac{2\pi k}{3C^2} \left[ \ln^2 \frac{C - X_\infty}{C + X_\infty} + \left( \frac{\pi}{2} \right)^2 \right], \quad C > X_\infty, \quad (40)$$

$$\frac{\varepsilon_s}{k^3 V_{\text{tot}}} = \frac{2\pi k}{3C^2} \left[ \ln^2 \frac{X_\infty - C}{X_\infty + C} + \delta^2 \frac{4C^2}{(X_\infty^2 - C^2)^2} \right], \quad C < X_\infty. \quad (41)$$

Note that  $\varepsilon_e$  is proportional to  $V_{\text{tot}}$ . Therefore the total power of scattered light depends on how the soot material is divided among individual clusters, assuming that the total concentration of the soot material in the scattering volume is fixed. When  $C > X_\infty$  the long-wavelength asymptote for the specific scattering is  $\varepsilon(\lambda) \propto 1/\lambda^4$ . In the opposite case ( $C < X_\infty$ ), the asymptote is more complicated and includes two competing terms,  $\propto 1/\lambda^4$  and  $\propto 1/\lambda^6$ . The latter term is characteristic of noninteracting monomers and is dominating in the limit  $C \rightarrow 0$  or  $\gamma \rightarrow \infty$ , when the mean-field approximation becomes accurate.

#### 4. SUMMARY AND DISCUSSION

We have built a theory of long-wavelength optical properties of fractal clusters with optical constants that are dominated by the input of free electrons in the  $\lambda \rightarrow \infty$  limit. Analytical expressions were derived for the extinction and scattering cross sections. The theory was applied to fractal carbonaceous soot, and the results were verified by comparison with experimental measurements in a wide spectral range.

Although a study of carbonaceous soot is the main focus of this paper, our approach is of a more general applicability. We made three main approximations, all of which proved to be highly accurate for the object under investigation but are essentially independent of one another. These approximations are (i) the geometrical renormalization of clusters, (ii) the quasi-static approximation, and (iii) replacing the weighted density of states (WDS) with a step function.

The geometrical cluster renormalization method (GCRM) is applicable beyond the quasi-statics when the retardation effects are fully included in the consideration. It also does not put any explicit restrictions on the geometry of samples (as long as they are fractal with  $D < 3$ ) or the refractive index of the material, although this subject has been insufficiently investigated so far. The quasi-static approximation is, clearly, applicable when the clusters are small compared with the wavelength but can also

be highly accurate in large clusters with low fractal dimensions<sup>12</sup> because the near-zone EM interaction is fast decaying as  $1/r^3$ . Finally, the step-function approximation is applicable only when certain mathematical relations between the WDS and the complex spectral variable  $1/\chi$  hold. Thus, this approximation puts restrictions on the refractive index, the geometry, or both. However, it can be applied beyond the quasi-static limit, although the analytical expressions in this case become more cumbersome.

We showed that the asymptotic form of the specific extinction  $\varepsilon_s(\lambda)$  in the limit  $\lambda \rightarrow \infty$  can be either  $1/\lambda$  or  $1/\lambda^2$ . The crossover between these two regimes has the nature of a critical phenomenon and is governed by the parameter  $vw_0$  that characterizes the effective width of the WDS. We have identified the critical value of this parameter,  $(vw_0)_c$ .

#### ACKNOWLEDGMENTS

This research was supported by the Battelle Institute under contract DAAH04-96-C-0086. It was also partially supported by the National Computational Science Alliance (NCSA) under grant PHYN980006N (and utilized the NCSA HP/Convex Exemplar SPP-2000), by the National Science Foundation under grant DMR-9810183 and by the U.S. Army Research Office under grant DAAG55-98-1-0425). The authors are grateful to C. Bruce for very useful discussions and to D. Mackowski for making available his Fortran codes.

The author's e-mail address is vmarkel@ee.wustl.edu.

#### REFERENCES AND NOTES

1. S. R. Forrest and T. A. Witten, "Long-range correlations in smoke-particle aggregates," *J. Phys. A* **12**, L109-L117 (1979).
2. H. X. Zhang, C. M. Sorensen, E. R. Ramer, B. J. Olivier, and J. F. Merklin, "In situ optical structure factor measurements of an aggregating soot aerosol," *Langmuir* **4**, 867-871 (1988).
3. U. O. Koylu and G. M. Faeth, "Structure of overfire soot in buoyant turbulent diffusion flames at long residence times," *Combust. Flame* **89**, 140-156 (1992).
4. J. Cai, N. Lu, and C. M. Sorensen, "Comparison of size and morphology of soot aggregates as determined by light scattering and electron microscope analysis," *Langmuir* **9**, 2861-2867 (1993).
5. M. V. Berry and I. C. Percival, "Optics of fractal clusters such as smoke," *Opt. Acta* **33**, 577-591 (1986).
6. W. H. Dalzell and A. F. Sarofim, "Optical constants of soot and their application to heat-flux calculations," *Trans. ASME, Ser. C: J. Heat Transfer* **91**, 100-104 (1969).
7. G. W. Mulholland, C. F. Bohren, and K. A. Fuller, "Light scattering by agglomerates: coupled electric and magnetic dipole method," *Langmuir* **10**, 2533-2546 (1994).
8. D. W. Mackowski, "Electrostatics analysis of radiative absorption by sphere clusters in the Rayleigh limit: application to soot particles," *Appl. Opt.* **34**, 3535-3545 (1995).
9. C. W. Bruce, T. F. Stromberg, K. P. Gorton, and J. B. Mozer, "Trans-spectral absorption and scattering of electromagnetic radiation by diesel soot," *Appl. Opt.* **30**, 1537-1546 (1991).
10. L. S. Markel, V. A. Muratov, and M. I. Stockman, "Optical properties of fractals: theory and numerical simulation," *Sov. Phys. JETP* **71**, 455-464 (1990).
11. V. A. Markel, L. S. Muratov, M. I. Stockman, and T. F.

- George, "Theory and numerical simulation of optical properties of fractal clusters," *Phys. Rev. B* **43**, 8183–8195 (1991).
12. V. M. Shalaev, R. Botet, and R. Jullien, "Resonant light scattering by fractal clusters," *Phys. Rev. B* **44**, 12,216–12,225 (1991).
  13. V. M. Shalaev, *Nonlinear Optics of Random Media: Fractal Composites and Metal Dielectric Films* (Springer-Verlag, Berlin, 2000).
  14. J. M. Gerardy and M. Ausloos, "Absorption spectrum of clusters of spheres from the general solution of Maxwell's equations. The long-wave limit," *Phys. Rev. B* **22**, 4950–4959 (1980).
  15. F. Claro, "Absorption spectrum of neighboring dielectric grains," *Phys. Rev. B* **25**, 7875–7876 (1982).
  16. R. Rojas and F. Claro, "Electromagnetic response of an array of particles: normal-mode theory," *Phys. Rev. B* **34**, 3730–3736 (1986).
  17. K. A. Fuller, "Scattering and absorption cross sections of compounded spheres. I. Theory for external aggregation," *J. Opt. Soc. Am. A* **11**, 3251–3260 (1994).
  18. F. J. G. de Abajo, "Interaction of radiation and fast electrons with clusters and dielectrics: a multiple scattering approach," *Phys. Rev. Lett.* **82**, 2776–2779 (1999).
  19. F. J. G. de Abajo, "Multiple scattering of radiation in clusters of dielectrics," *Phys. Rev. B* **60**, 6086–6102 (1999).
  20. J. E. Sansonetti and J. K. Furdyna, "Depolarization effects in arrays of spheres," *Phys. Rev. B* **22**, 2866–2874 (1980).
  21. F. Claro, "Theory of resonant modes in particulate matter," *Phys. Rev. B* **30**, 4989–4999 (1984).
  22. F. Claro, "Multipolar effects in particulate matter," *Solid State Commun.* **49**, 229–232 (1984).
  23. V. A. Markel, V. M. Shalaev, E. B. Stechel, W. Kim, and R. L. Armstrong, "Small-particle composites. I. Linear optical properties," *Phys. Rev. B* **53**, 2425–2436 (1996).
  24. V. A. Markel and V. M. Shalaev, "Computational approaches in optics of fractal clusters," in *Computational Studies of New Materials*, D. A. Jelski and T. F. George, eds. (World Scientific, Singapore, 1999), pp. 210–243.
  25. E. A. Taft and E. A. Philipp, "Optical properties of graphite," *Phys. Rep.* **138**, A197–A202 (1965).
  26. Z. G. Habib and P. Vervisch, "On the refractive index of soot at flame temperatures," *Combust. Sci. Technol.* **59**, 261–274 (1988).
  27. S. C. Lee and C. L. Tien, "Optical constants of soot in hydrocarbon flames," in *Eighteenth Symposium (International) on Combustion*, (The Combustion Institute, Pittsburgh, Pa., 1981), pp. 1159–1166.
  28.  $X$  and  $\delta$  used in Refs. 11 and 10 differ from the dimensionless parameters defined below by a multiplicative factor with the dimensionality of length cubed.
  29. D. W. Mackowski, "Calculation of total cross sections of multiple-sphere clusters," *J. Opt. Soc. Am. A* **11**, 2851–2861 (1994).
  30. P. Meakin, "Formation of fractal clusters and networks by irreversible diffusion-limited aggregation," *Phys. Rev. Lett.* **51**, 1119–1122 (1983).
  31. R. Jullien, M. Kolb, and R. Botet, "Aggregation by kinetic clustering of clusters in dimensions  $d > 2$ ," *J. Phys. (France)* **45**, L211–L216 (1984).
  32. B. T. Draine, "The discrete-dipole approximation and its application to interstellar graphite grains," *Astrophys. J.* **333**, 848–872 (1988).
  33. E. M. Purcell and C. R. Pennypacker, "Scattering and absorption of light by nonspherical dielectric grains," *Astrophys. J.* **186**, 705–714 (1973).
  34. B. Draine and P. Flatau, "Discrete-dipole approximation for scattering calculations," *J. Opt. Soc. Am. A* **11**, 1491–1499 (1994).
  35. V. A. Markel, "Coupled-dipole approach to scattering of light from a one-dimensional periodic dipole chain," *J. Mod. Opt. Soc. Am. B* **40**, 2281–2291 (1993).
  36. A finite linear chain of touching spheres with multipole interaction was considered by Mackowski.<sup>8</sup> It was found numerically that, in general, such a chain is not equivalent to a spheroid with the same aspect ratio. The intersection parameter that gives the same depolarization coefficient for an infinite chain of spheres as in an infinite cylinder may be different with the multipole interactions included from that in the dipole approximation.
  37. V. A. Markel, "Scattering of light from two interacting spherical particles," *J. Mod. Opt.* **39**, 853–861 (1992).
  38. V. A. Markel, "Antisymmetrical optical states," *J. Opt. Soc. Am. B* **12**, 1783–1791 (1995).
  39. T. A. Witten and L. M. Sander, "Diffusion-limited aggregation, a kinetic critical phenomenon," *Phys. Rev. Lett.* **47**, 1400–1403 (1981).